Coherent Transport of Atomic Quantum States in a Scalable Shift Register

A. Lengwenus,[1] J. Kruse,[1] and G. Birkl[1,*]

[1] *Institut für Angewandte Physik, Technische Universität Darmstadt, 64289 Darmstadt, Germany*

(Dated: March 4, 2009)

The coherent storage and transport of atomic quantum systems in versatile potential geometries are key elements for the investigation of quantum information processing and quantum degenerate gases. In this work we present the controlled coherent transport of two-dimensional arrays of small ensembles of neutral atoms in a register-type geometry based on two-dimensional arrays of microlenses. We show the scalability of our architecture and of the transport process by demonstrating the repeated hand-over of atoms from trap to trap. We investigate the processes of transport and reloading in detail and demonstrate the conservation of coherence during transport.

PACS numbers: 37.10.Jk, 42.50.Ct, 03.67.-a

Versatile architectures for the coherent storage and transport of atomic quantum systems play a crucial role in many of the most dramatic recent advances in the physics of quantum degenerate gases and quantum information processing. Due to their high flexibility, optical trapping geometries based on dipole forces are central in this respect. In specific, the application of single or multiple focused laser beams [1, 2, 3] and standing-wave configurations [4, 5, 6, 7] has led to significant progress in the manipulation of atomic qubit states for quantum information processing. In our work, we focus on the implementation of geometries based on microfabricated optical elements [8, 9, 10, 11]. This approach allows us to develop flexible and integrable configurations for quantum state storage and manipulation, simultaneously targeting the important issues of single-site addressing and scalability, essential to every successful architecture for quantum informaton processing [12].

The scalable shift register presented here is an all optical device which offers precise control of the position of trapped neutral atoms. The atoms are localized in miniaturized arrays of dipole potentials created by microfabricated lens structures [9]. The shift operation is based on consecutive loading, moving and reloading of two independently controllable arrays of traps. Figure 1 shows a two-dimensional register of about 25 atom samples after 0, 1, 2, and 3 consecutive shift sequences detected by collecting the fluorescence light emitted by the atoms when illuminated with a resonant laser pulse. The shift register allows atom transport over macroscopic distances and at the same time fulfills the stringent requirements for controlled atom-atom interactions, like two-qubit quantum gates for trapped atoms [13, 14, 15, 16, 17, 18]. It allows to approach atoms with sub-micrometer precision while having complete control over the interaction sequence and timing [19]. Moreover, it can serve as a two-dimensional quantum memory to archive and retrieve information, or sequentially shuffle quantum information through complex architetures. Conservation of coherence of the quantum states and adiabaticity during transport are essential requirements that will be addressed in this paper.

The experiments presented here are performed with ^{85}Rb atoms inside a glass cell based vacuum system (Fig. 2). Each experimental sequence is initiated by preparing an ensemble of about 10^6 atoms in a standard retroreflected magneto-optical trap (MOT). The atoms are further cooled by optical molasses to approximately 10 µK before being partially transferred into a superimposed register of dipole traps. The traps are created by illuminating a subset of a two-dimensional array (A1) of 50×50 microfabricated refractive lenses with light far red-detuned from the D1 and D2 transitions of Rb. The microlenses have a diameter of 100 µm, a pitch of 125 µm, and a focal length of 1 mm. The focal plane of the array is relayed into the glass cell using a telescope which consists of an achromatic lens (L1, $f = 80$ mm) and a diffraction limited lens system (LS) with a focal length of 35.5 mm and $NA = 0.29$. This demagnification results in traps with a separation of $a = 55$ µm and a measured waist of 3.8 µm ($1/e^2$ radius). Illuminating the microlens array with laser light at 805 nm wavelength, a power of 275 mW, and a beam waist of 450 µm, results in a two-dimensional register of traps with a depth of the central trap of $k_\mathrm{B} \times 450$ µK. Here, the vibrational frequencies are $\nu_\mathrm{r} = 18$ kHz for the radial and $\nu_\mathrm{a} = 750$ Hz for the axial direction. About 200 atoms with a temperature of 15 ± 1.5 µK (measured

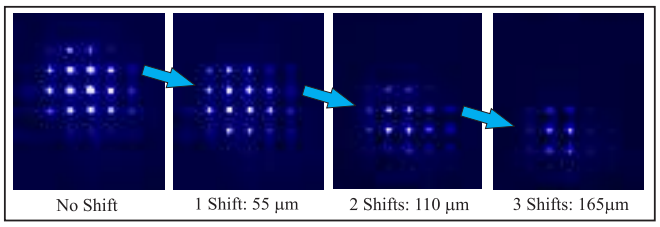

FIG. 1: (color online) Fluorescence images of two-dimensional arrays of trapped atoms in a shift register based on microlens arrays. Images are taken after 0, 1, 2, and 3 consecutive shift sequences of 55 micron transport distance each.

by a time-of-flight technique) are trapped in the central trap. Because of the Gaussian profile of the laser beam illuminating the microlens array, the outlying traps are shallower and the number of traps loaded depends on this beam size but also on the size of the MOT. The lifetime of the atoms in the traps is on the order of 500 ms which is mainly limited by collisions with background gas atoms. Atom detection is achieved by resonance fluorescence imaging of the atom distribution using the MOT beams for illumination and collecting the fluorescence light with an EMCCD camera through lens system LS and beamsplitter BS1.

To move the traps, we vary the incident angle on microlens array A1 by an actively controlled scanning mirror S which deflects the incoming beam. The pivot point of the beam on the scanning mirror is imaged onto the microlens array by telescope L2 with unity magnification. This causes the foci of the array to shift sideways within the focal plane as a function of the angle of the scanning mirror. It is possible to shift the array by a distance of the full trap separation of 55 µm. Moving significantly more than this distance results in strong deformations of the trapping potentials by lens abberations due to the skewed illumination of the microlenses. The angular repeat accuracy of the scanner is better than 22 µrad which guarantees that the trap position can be controlled with an accuracy of better than 10 nm.

A complete shift register sequence consists of consecutive loading, moving, and reloading of two independently controllable arrays of dipole traps. The fixed focal plane of microlens array A2 (identical to lens array A1) is

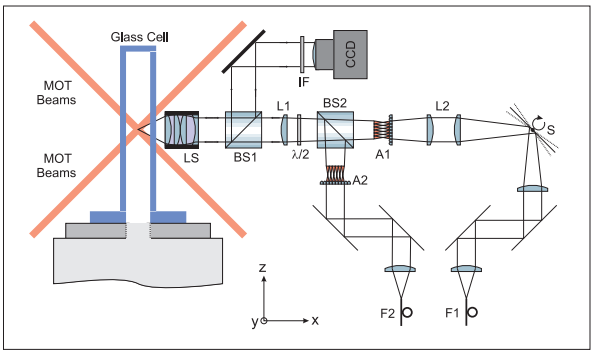

FIG. 2: (color online) Experimental setup for transporting atoms in arrays of dipole traps. Microlens array A1 is illuminated by the light of a TiSa laser delivered by optical fiber F1. The incident angle on A1 is changed by scanning mirror S in combination with the transfer lenses L2. A second fixed array A2 is illuminated with light delivered by fiber F2. Both focal planes are superimposed by beamsplitter BS2 and transferred by lens L1 and lens system LS into the MOT region. Detection of fluorescence light is performed through LS and beamsplitter BS1 by a CCD camera. Straylight from the dipole trap lasers is blocked by interference filter IF.

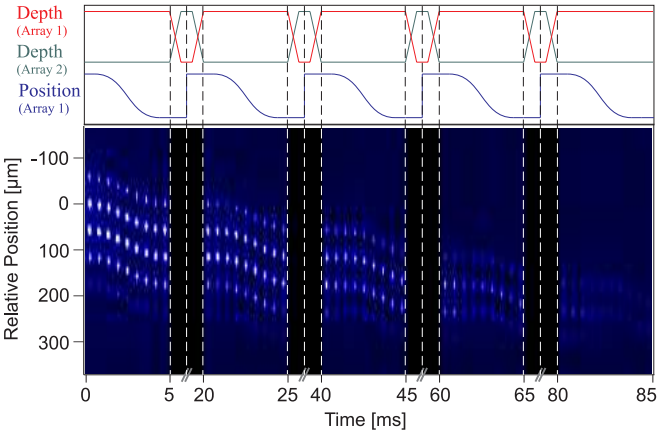

FIG. 3: (color online) (top) Timing sequence for depth and position of the two trap arrays constituting a shift register. (bottom) Fluorescence images of atoms in the central column of the register of Fig. 1 during 5 consecutive transport cycles. No images are shown for the two phases of loading between the arrays and the phase of returning array A1 (5 ms each).

combined with the movable focal plane of array A1 by beamsplitter BS2. For an optimized overlap of the traps, array A2 is illumated under a fixed, non-normal angle which displaces the focal plane by $+a/2$ and array A1 shifts its focal plane between $-a/2$ and $+a/2$. The shift sequence is comparable to a bucket chain (Fig. 3): while the fixed array is switched off initially, we load atoms from the MOT into the moveable array and shift the array by one full trap separation ($-a/2$ to $+a/2$) in a few ms. We transfer the atoms to the fixed array by rising the intensity in the fixed array while ramping it down in the moveable array. Now the scanning mirror is returned to its initial position. The atoms are reloaded from the fixed array into the movable array and the next shift sequence begins. For shift and reloading durations of 5 ms, the timing sequence for the potential depths of arrays A1 and A2 and for the position of array A1 are shown in Fig. 3 (top). The fluorescence images in Fig. 3 (bottom) show the central column of the array of Fig. 1 as a function of time during 5 consecutive transfer periods giving a final transfer distance of 275 µm. The number of transfer sequences is limited by the size of the illuminated trap array (5×5 traps in this realization). Using the full available set of 50×50 microlenses, atom transport over a distance of 2.7 mm in one or two dimensions is achievable for sufficent laser power.

In most applications, heating and atom loss have to be minimized during transport. Heating results from transitions to higher vibrational states of the trap, and is mainly induced by fast, non-adiabatic displacement and deformation of the trapping potential. Minimizing heating and loss is not only essential for the full shift register, but already for elementary processes, like single transport operations or specific classes of quantum gates

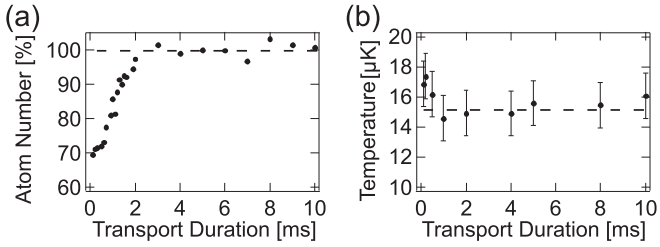

FIG. 4: (a) Atom number and (b) temperature at the end of a single transport sequence of 55 micron distance for different transport durations. The dashed line in (b) shows the temperature for a fixed trap. Each data point results from averaging 15 individual realizations.

[13, 14, 15, 16, 17, 18], where the atoms have to be brought close together and separated again. For that reason, we investigated in detail heating and atom loss during individual transport operations. Figure 4 shows atom number and temperature at the end of single transport sequences with varying duration. The transfer distance is one full trap separation. Typical initial temperatures are 15 ± 1.5 μK. For transport durations above 1 ms we measure no increase in temperature and for transport durations above 2 ms no atom loss. The reason for heating and atom loss for fast transport arises from technical limitations of the scanning mirror: for short scanning times the mirror has to be strongly accelerated and decelerated. For decelerations too strong, the mirror overshoots its final position because of its inertia. This results in oscillations around the final position which cause resonant excitation of the vibrational levels and as a consequence heating and atom loss. Optimization allowed us to minimize this effect by smoothing the ramps for acceleration and deceleration as shown in the trace for the position of array A1 in Fig. 3 (top).

We also investigated heating and atom loss for the complete shift register consisting of several transport and reloading cycles. For the sequence of Fig. 3 with transfer and reloading durations of 5 ms each, heating was measured to be below 2 μK after four shift cycles, which is comparable to our measurement uncertainty. Atoms can be reloaded between traps without observable loss within our measurement uncertainty when the traps are matched in size. For imperfectly matched traps, we still could achieve lossless loading of atoms from a tighter to a wider trap but observed atom losses on the order of 20% for loading atoms from wider ot a tighter trap. In order to minimize a mismatch in trap size, we symmetrized the loading and reloading processes for the complete shift register by having the focal planes of both arrays displaced simultaneously by $|+a/2|$ at the reloading phase as described above.

In order to use our architecture for quantum information processing, e.g. for building two-qubit gates via atom-atom interactions, the transport process also has to preserve the coherence of superpositions of internal states of the transported atoms. In our approach, qubit states are represented by hyperfine substates of the $5S_{1/2}$ ground state of ^{85}Rb. To be insensitive to fluctuations of magnetic fields to first order, we prepare the atoms in the clock state ($F = 2$, $m_F = 0$) and coherently couple it to the second clock state ($F = 3$, $m_F = 0$) with a phase-locked Raman laser system. The typical duration of an applied π-pulse is 210 μs. State-selective detection is performed by removing the atoms in $F = 3$ by a laser pulse which is resonant to the $F = 3 \rightarrow F = 4$ transition and subsequent detection of the remaining atoms in $F = 2$.

We analyze the influence of atom transport on dephasing and decoherence by applying Ramsey and spin-echo methods (Fig. 5) [20, 21]. The trapping laser is tuned to 815 nm with an power of 150 mW distributed over a beam with a waist of 520 μm. This gives a trap depth of $k_B \times 100$ μK in the central trap. As the atom ensemble in each trap is thermal and thus distributed over a range of vibrational levels, each atom incurs a slightly different ac-Stark shift. This leads to inhomogeneous dephasing of the Ramsey signal with time constants comparable to the transport duration. To compensate for this we implemented a spin-echo technique [21] which allows us to measure the combined time constant for homogeneous dephasing and decoherence and to perform a direct comparison between atoms at rest and atoms transported. For atoms at rest, a $\pi/2$-pulse at $t = 0$ is followed by a first period of free evolution. Rephasing is induced by a π-pulse after t_π. After an additional period of free evoluton with variable duration, the sequence is completed by a second $\pi/2$-pulse and detection of the atoms in $F = 2$. The maximum amplitude of the echo signal occurs at $t = 2t_\pi$ (Fig. 5 (a) with $2t_\pi = 20$ ms). For the case of transported atoms, transport over a

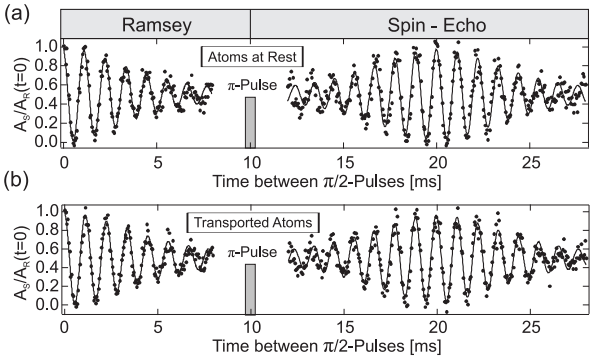

FIG. 5: Typical Ramsey and spin-echo measurements atoms at rest (a) and transported atoms (b) in the central trap of a two-dimensional trap array. There is almost negligible additional loss of signal contrast for transported atoms. Each data point results from averaging 5 indiviual realizations.

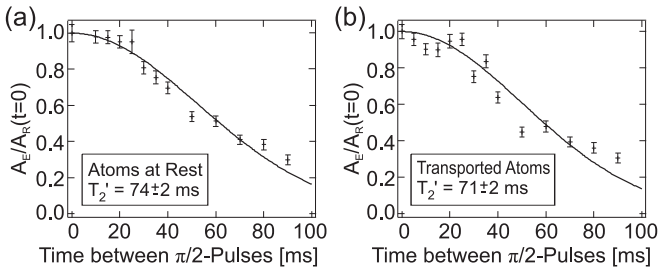

FIG. 6: Determination of the time constants for homogeneous dephasing for atoms at rest (a) and atoms transported in 2 ms (b). Atom transport only causes a minor increase in homogeneous dephasing, still within our measurement uncertainty.

distance of 55 µm takes place during the first 2 ms of the first period of free evolution with no transport during the second period of free evolution (Fig. 5 (b)). Additional dephasing and decoherence caused by atom transport are not compensated during the second period of free evolution and should cause a reduction of the signal amplitude. Fig. 5 shows that this effect is almost neglible in our system.

For a quantitative investigation, Fig. 6 presents the signal contrast, i.e. the amplitude of the echo signal A_{E} normalized to the amplitude of the Ramsey signal $A_{\mathrm{R}}(t=0)$, as a function of $2t_\pi$ for atoms at rest (a) and atoms transported over 55 µm within 2 ms (b). The loss in signal contrast is clearly non-exponential. From a detailed analysis of external influences, we determine homogeneous dephasing due to irreversible variations of the atomic resonance frequency with time-independent variance σ_{freq} to be the dominant cause of loss of contrast. We identify heating due to photon scattering from the trapping laser with a heating rate too small to be directly observable in Fig. 4 to be the most likely cause. Following the calculations for homogeneous dephasing given in [22] the signal contrast is described by a Gaussian function: $C(2t_\pi) = C_0 \exp(-t_\pi^2 \sigma_{\mathrm{freq}}^2/2)$. The homogeneous dephasing time T_2' is defined by $T_2' = \sqrt{2}/\sigma_{\mathrm{freq}}$. For the measurements in Fig. 6 this gives a homogeneous dephasing time of $T_2' = 74 \pm 2$ ms for atoms at rest and $T_2' = 71 \pm 2$ ms for atoms transported. Atom transport only causes a minor decrease in T_2', even being consistent with 0 within our measurement uncertainty. This proofs that coherence remains conserved to a high degree even during atom transport.
With the spin-echo technique, we also can detect phase shifts in the coherent evolution for atoms transported relative to atoms at rest [2]. For a transport time of 2 ms the phase shift $\Delta\phi = 0.1\pi$. This phase shift is caused by a variation of the trap depth during transport due to small changes in the achievable spot size as a function of the illumination angle. During transport, the atoms spend some time in the slightly deeper potentials created at an illumination of the microlens array at normal incidence. This results in the observed phase shift which is reproducible and can be kept at a minimum for sufficiently fast transport or even can be compensated for by keeping the trap depth constant through a matched temporal variation of the illumination intensity.
In summary, in this paper we have presented a versatile and scalable two-dimensional architecture for the transport of atomic quantum systems based on arrays of microfabricated lenses. We have demonstrated a novel shift register and the resulting transport of atomic qubits without atom loss, heating, and with negligible additional dephasing and decoherence. Together with the ability of parallelized site-selective single atom detection [23] this approach allows the development of flexible geometries for coherent single atom storage and manipulation, specifically addressing the important issue of scalability, essential to every successful architecture for quantum informaton processing.
We acknowledge financial support by the DFG, by the European Commission (IP SCALA), by NIST (award 60NANB5D120), and by the DAAD (contract 0804149).

* Electronic address: gerhard.birkl@physik.tu-darmstadt.de

[1] D. D. Yavuz et al., Phys. Rev. Lett. **96**, 063001 (2006).
[2] J. Beugnon et al., nature physics **3**, 697 (2007).
[3] M. P. A. Jones et al., Phys. Rev. A **75**, 040301 (2007).
[4] S. Kuhr et al., Science **293**, 278 (2001).
[5] O. Mandel et al., Nature (London) **425**, 937 (2003).
[6] Y. Miroshnychenko et al., Nature (London) **442**, 151 (2006).
[7] M. Anderlini et al., Nature (London) **448**, 452 (2007).
[8] G. Birkl, R. Dumke, F. B. Buchkremer, and W. Ertmer, Opt. Comm. **191**, 67 (2001).
[9] R. Dumke et al., Phys. Rev. Lett. **89**, 097903 (2002).
[10] R. Dumke, T. Müther, M. Volk, W. Ertmer, and G. Birkl, Phys. Rev. Lett. **89**, 220402 (2002).
[11] A. Lengwenus, J. Kruse, M. Volk, W. Ertmer, and G. Birkl, Appl. Phys. B **86**, 377 (2007).
[12] D. P. DiVincenzo, Fortschritte der Physik **48**, 771 (2000).
[13] G. K. Brennen, C. M. Caves, P. S. Jessen, and I. H. Deutsch, Phys. Rev. Lett. **82**, 1060 (1999).
[14] D. Jaksch, H.-J. Briegel, J. I. Cirac, C. W. Gardiner, and P. Zoller, Phys. Rev. Lett. **82**, 1975 (1999).
[15] D. Jaksch et al., Phys. Rev. Lett. **85**, 2208 (2000).
[16] K. Eckert et al., Phys. Rev. A **66**, 042317 (2002).
[17] J. Mompart, K. Eckert, W. Ertmer, G. Birkl, and M. Lewenstein, Phys. Rev. Lett. **90**, 147901 (2003).
[18] D. Hayes, P. S. Julienne, and I. H. Deutsch, Phys. Rev. Lett. **98**, 070501 (2007).
[19] T. Calarco et al., Phys. Rev. A **61**, 022304 (2000).
[20] N. Ramsey, Molecular Beams (Ox. Univ. Press) (1956).
[21] E. Hahn, Phys. Rev. **80**, 580 (1950).
[22] S. Kuhr et al., Phys. Rev. A **72**, 023406 (2005).
[23] J. Kruse et al., to be published (2009).